Dynamic Changes of Acoustic Load and Complex Impedance as Reporters for the Cytotoxicity of Small Molecule Inhibitors

ARTICLE *in* CHEMICAL RESEARCH IN TOXICOLOGY · AUGUST 2011

Impact Factor: 3.53 · DOI: 10.1021/tx200115q · Source: PubMed

6 AUTHORS, INCLUDING:

Eva Sunnick
Gesellschaft für wissenschaftliche Datenvera…
13 PUBLICATIONS **226** CITATIONS
SEE PROFILE

David Schneider
Max Planck Institute for Biology of Ageing
12 PUBLICATIONS **196** CITATIONS
SEE PROFILE

Angelika Kunze (Sapper)
Georg-August-Universität Göttingen
21 PUBLICATIONS **173** CITATIONS
SEE PROFILE

Andreas Janshoff
Georg-August-Universität Göttingen
204 PUBLICATIONS **5,612** CITATIONS
SEE PROFILE

Chemical Research in Toxicology

ARTICLE

pubs.acs.org/crt

Dynamic Changes of Acoustic Load and Complex Impedance as Reporters for the Cytotoxicity of Small Molecule Inhibitors

Marco Tarantola,[†] Eva Sunnick,[‡] David Schneider,[‡] Anna-Kristina Marel,[§] Angelika Kunze,[∥] and Andreas Janshoff*[,‡]

[†]Max Planck Institute for Dynamics and Self-Organization, Laboratory for Fluid Dynamics, Pattern Formation and Nanobiocomplexity (LFPN), Fassberg 17, D-37077 Goettingen, Germany

[‡]Institute of Physical Chemistry, University of Goettingen, Tammannstrasse 6, D-37077 Goettingen, Germany

[§]Department of Physics, Ludwig-Maximilians-University Munich, Geschwister-Scholl-Platz 1, D-80539 Muenchen, Germany

[∥]Department of Applied Physics, Chalmers University of Technology, SE-412 96 Goeteborg, Sweden

Supporting Information

ABSTRACT: Cellular motility is the major driving force of numerous biological phenomena including wound healing, immune response, embryogenesis, cancer formation, and metastasis. We studied the response of epithelial FaDu monolayers cultured on gold electrodes of an acoustic resonator (quartz crystal microbalance, QCM) and impedance sensor (electric cell−substrate impedance sensing, ECIS) to externally applied chemical stimuli interfering with cytoskeleton organization. Epithelial cell motility of confluent monolayers is characterized by subtle cell shape changes and variations in the cell−substrate as well as cell−cell distance without net directionality of individual cells. The impact of small molecules such as cytochalasin D, phalloidin, and blebbistatin as well as paclitaxel, nocodazol, and colchicin on actin and microtubules organization was quantified by conventional sensors' readouts and by comparing the noise pattern of the signals which is attributed to cellular dynamics. The responsiveness of noninvasive and label-free techniques relying on cellular dynamics is compared to classical viability assays and changes of the overall impedance of ultrasmall electrodes or acoustic loads of a thickness shear mode resonator. Depending on the agent used, a distinct sensor response was found, which can be used as a fingerprint of the cellular response. Cytoskeletal rearrangements and nuclear integrity were corroborated by fluorescence microscopy and correlated to the readouts of QCM and ECIS.

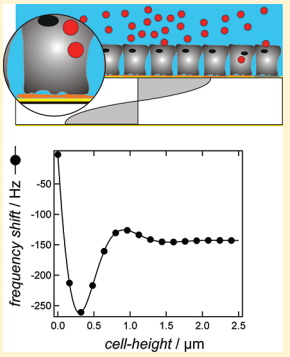

INTRODUCTION

An essential activity of malignant, invading cells is migration.[1] Epithelial tumor cells, the prevalent origin of malignancies, translocate by remodeling of cell−cell as well as cell−matrix contacts and reorganization of the extracellular matrix.[2] The source of the net vertical cell migration in epithelial monolayers is the dynamics of biopolymer assembly and disassembly of the cytoskeleton and accessory proteins[3,4] in the cytosol as well as in membrane proximity.[5] Cellular dynamics is primarily governed by the actin networks[6] with fibers and bundles building protrusions[7] as well as by microtubules, which partially control actin activity[8] and present a dynamic instability for fast network reorganization.[9] Intermediate filaments contribute only to the static, mechanical stabilization of the cell and therefore play a less important role in the vertical motility of adherent cells.[10,11] Additionally, regulatory Rho-GTPases orchestrate cellular migration, with RAC1 controlling extensions and new anchorage sites, CDC42 supervising cell polarity, and rhoA mediating cell adhesion through integrins and motility via actin−NMII contractions.[12] This dynamic cellular migration assembly is not restricted to cancer neoplasia but also found in normal, healthy cells.[13]

Label-free, noninvasive biosensors, which capture the inherent dynamics of living cells to report on their biological activity and vitality, extend the information content of classical biochemical cytotoxicity assays. More recently, the noise originating from adherent cells has been used to assess the dynamic properties of cellular ensembles giving rise to collective fluctuations mirrored in the time trace of the sensor. The micromotion of cells measured by resistance or acoustic load fluctuations is frequently used to quantify cell vitality in addition to conventional cytotoxicity assays.[14−17]

In this work, we investigated to what extent biological noise produced by collective vertical motion of confluent cell-monolayers is affected by small molecule inhibitors that affect cytoskeleton organization. Both, viscoelastic and shape changes are detected by means of the quartz crystal microbalance with dissipation monitoring (D-QCM) reporting on the acoustic load of a Thickness-Shear-Mode (TSM)-resonator and Electric Cell-Substrate Impedance Sensing (ECIS) that measures time-dependent changes in impedance as a function of applied frequency. The time-resolved data was correlated with fluorescence microscopy to document structural changes accompanying exposure to the various toxins. Despite the frequent use of these

Received: March 14, 2011
Published: August 04, 2011

sensors to document the biological activity of cells in response to external stimuli, a systematic study of correlation between sensor output and cellular responses is lacking. Hence, the major goal of this study is to correlate sensor responses with cytoskeleton dynamics by selective perturbation of actin filaments, microtubules, and myosin II. Particularly, we try to provide a recommendation as to the cases in which dynamic parameters derived from fluctuation analysis are superior over the conventional assessment of acoustic load or electrical impedance of cell covered electrodes.

QCM and ECIS are frequently employed biosensors for adherent cells.[15,16,18−22] Single cells or confluent monolayers are thereby cultured on gold electrodes integrated in culture vessels. While ECIS measurements provide spectral information of the complex resistance Z, QCM displays changes in acoustic load often divided into deposited mass and energy dissipation represented by changes in resonance frequency f and dissipation δ. A broad range of biological and medical applications of QCM and ECIS exists,[23] often involving modulators of cellular micromechanics such as adhesion under nocodazol influence (QCM),[24] viscoelasticity modulated by a variety of drugs including actin polymerizing jasplakinolide and paclitaxel (QCM),[25] cellular attachment upon cytochalasin D treatment (QCM),[26] toxicity of cisplatin, or other metal compounds (ECIS)[27] as well as its chemotherapeutic, apoptotic effect on cancer cells.[28,29] So far, the focus lies exclusively on static rather than the dynamic features of adherent living cells hidden in the inherent fluctuations of motile cells. Recently, we proved that noise produced by adherent cells on quartz resonators can be employed to categorize the invasive behavior of cancer cells or to measure the toxicity of nanoparticles.[17]

The goal of the current study is to systematically study and classify the impact of toxins addressing the cytoskeleton of epithelial cells on the sensors' responses with particular emphasis on the changes in fluctuation amplitude and long-term memory.

MATERIALS AND METHODS

Cell Culture. FaDu cells,[30] a squamous carcinoma cell line derived from the hypopharynx, is cultured in Dulbecco's modified Eagle's medium with 4.5 g/L glucose and 2 mM L-glutamine (PAA laboratories GmbH, Cölbe, Germany), nonessential amino acids NEA (100 μg/mL), sodium pyruvate (1 mM), and 10 mM HEPES buffer. Both cell lines are cultured in incubators (HERA cell 150, Heraeus, Germany) with a 5% CO_2 atmosphere. Cells are subcultured weekly after reaching confluence by washing with PBS, followed by trypsinization and centrifugation at 110 × g. Counting is carried out using a Buerker-chamber, and viability is determined using trypan blue exclusion. The passage number is typically kept between 20 and 40 to ensure that the neoplastic phenotype did not change during the experiments.

Cells are seeded at a density of 6−7 × 10^5 cells/mL directly onto QCM quartzes or in the 8-well ECIS electrode arrays as described previously.[16] Fixation of cells is carried out using 0.5% (v/v) glutardialdehyde (GDA) (Sigma-Aldrich, Germany) solution, and exchange of medium with toxins is carried out upon reaching confluence, i.e., 15−24 h after seeding.

D-QCM Based Viscoelastic Monitoring and Noise Analysis. Changes in resonance frequency and dissipation are monitored using a D-QCM setup as described previously.[31] Both fluctuation in frequency and dissipation were analyzed by Fourier analysis and computation of variance.[14] In brief, time series of frequency and dissipation are detrended and subjected to fast Fourier transformation (FFT) providing power spectra densities (PSD). The slope m of the PSD was determined in the low frequency regime as a function of time assuming stationarity of m in this interval. In fact, m represents the long-term memory of the time traces and can be assigned to cellular viability. Time series of the variance and FFT-slope were smoothed with adjacent averaging over four consecutive points assuming sufficient stationarity. Mean values of the 0−24 h interval (n = 12, ± SD) and the interval from 24 h to the end of experiment (24−72 h) are presented after normalization of m to the values for untreated cells for both viscoelastic and fluctuation parameters. All experiments were carried out at least in triplicate. Both variance and PSD slopes were standardized with respect to fixated cells. In order to distinguish between the conventional readout parameters such as f and δ and the noise-related parameters, we refer to F-QCM if the dynamic output of the D-QCM is employed. The noise amplitude was computed by computation of variance.[14]

ECIS Based Impedance Monitoring and Noise Analysis. Micromotion was determined from temporal changes of the in-phase voltage sampled at 4 kHz. The linearly detrended impedance fluctuations were subjected to FFT, and the slope of the low frequency regime of the PSD is used as a measure for micromotion. Noise amplitude was assessed by variance as described before.[14,16,18] $|Z|$ and fluctuation parameters (micromotion PSD-slope and variance) were normalized to levels found for untreated cells before toxin addition and standardized to the signal gained from a cell-free electrode. All kinetic experiments were carried out in triplicate.

Cytotoxicity Assay. The MTS cytotoxicity test was applied according to the manufacturer's protocol (Promega, Mannheim, Germany). Briefly, epithelial cells were grown to a predetermined optimal number of 12,000 cells/well in a 96-well plate and subsequently incubated with the toxic solution for 24 h. Thereafter, washing was carried out with full medium before adding 20 μL of MTS agent to 100 μL of medium-containing wells. Control experiments were carried out using cell-free wells or Triton-X-100 permeabilized cells with 1% (v/v) Triton-X-100. Cells were incubated for 45 min, and absorbance is determined at 490 nm. The color change is a direct measure of the cell's metabolic activity due to the reduction of MTS educts to formazan. Experiments were repeated three times and data pooled for determination of IC_{50} of testing solutions for biosensor experiments. DMSO solvent controls for FaDu cells yielded IC_{50} values of (6.8 ± 1.5) % (v/v) (n = 3). Toxin dilutions were kept reasonably below this regime.

Fluorescence Microscopy. Immunostaining, fluorescence, and bright field phase contrast microscopy were applied to visualize changes in the integrity of the cell cytoskeleton as well as overall morphological alterations. Therefore, cells were grown to confluence on Petri-dishes and afterward incubated with toxins at their corresponding IC_{50}. For actin and microtubules staining, washing with PBS and fixation/permeabilization was carried out by immersing the cells into a −20 °C cold acetone/methanol mixture (1:1 v/v) for 10 min. Afterward, the cells were washed three times with PBS, nonspecific binding sites saturated with FCS, and incubation in staining solutions carried out according to the manufacturer's recommendation: Alexa Fluor 546 phalloidin (Invitrogen, Paisley, UK) was used for f-Actin staining, Alexa Fluor-488-conjugated IgG1 anti-β-tubulin (BD Bioscience, Heidelberg, Germany) from mouse for labeling microtubules, 4′,6 diamidino-2-phenyindole (DAPI, Sigma-Aldrich, Seelze) for nucleus/DNA labeling, and monoclonal anti-ZO-1 or antioccluding rabbit antibody (Zymed Gmbh, Muenchen) followed by treatment with polyclonal Alexa Fluor-conjugated goat-anti rabbit IgG1 antibody (BD Bioscience, Heidelberg, Germany) for staining tight junctions proteins. Staining is carried out for 10 min (DAPI) or 30 min (Alexa) at room temperature, and cells are washed subsequently. Untreated cells served as controls and were stained correspondingly. An upright fluorescence microscope (Olympus BX51, 10, 40, or 100× water immersion (0.8 or 1.0 NA), Germany), equipped with a color camera (Olympus DP71), was used for visualization.

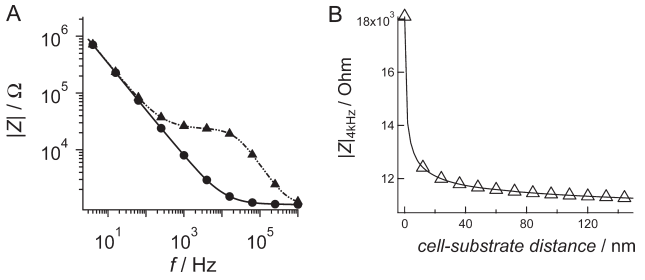

Figure 1. (A) Simulation of impedance spectra employing the model of Lo et al.[34] The uncovered electrode (●) is best described by a capacitance of constant phase element (C_{CPE} = 200 μF/cm^2, n = 8.2) in series to a resistance representing the electrolyte solution ($R_{specific}$ = 54 Ωcm). The impedance of the cell covered electrode (▲) is characterized by an ohmic behavior representing the barrier properties of the cells ($R_{barrier}$ = 10 Ωcm^2). The membrane capacitance was chosen to be 4 μF/cm^2, and α was set to 2.4 corresponding to a cell−substrate distance of 146 nm. (B) Change in impedance |Z| was recorded at a fixed frequency (4 kHz) as a function of the cell−substrate distance.

Sensor Principles. *Electric Cell−Substrate Impedance Sensing (ECIS).* The ECIS technique measures the complex impedance of two coplanar gold-electrodes electrically connected via the culture medium.[32−34] The electrodes allow cells to settle, adhere, and spread under ordinary cell culture conditions. Importantly, the two electrodes differ considerably with respect to their surface areas. The area of the counter electrode is about 1000 times larger than the size of the smaller working electrode (diameter of 250 μm). As a consequence, the impedance of the working electrode dominates the measured response and increases the sensitivity since cell-related changes in impedance are otherwise masked by the resistance of the bulk electrolyte.

In ECIS, impedance spectra are usually recorded in a frequency range between 1−10^6 Hz providing information about electrode coverage, cell−substrate distance, and barrier properties. Below 10 kHz for working electrodes of 250 μm in diameter, the cells behave essentially like insulating particles forcing the current to flow around the cell body paracellularly. Applying a sinusoidal voltage across the two electrodes results in a current flowing through the confined cleft between the ventral plasma membrane before it passes the paracellular shunt between adjacent cells into the bulk phase. Therefore, the impedance in this frequency regime provides information about the distance between cells and the electrode and the barrier properties of adjacent cell bodies. Modeling allows one to assign the individual impedance contributions either to the cell−substrate or the cell−cell contact sites.

At frequencies higher than 10 kHz, corresponding to an electrode size of 250 μm, the current can pass the cells directly since the impedance of the dielectric films is dominated by the capacitance of the ventral and dorsal membranes. For details, we refer to a more comprehensive review. [33]

Figure 1A shows a typical impedance spectrum modeling an electrode covered with a confluent cell monolayer in comparison to an uncovered electrode employing the area contact model of Lo et al.[34] We assumed a cell radius of 12.5 μm, a specific membrane capacitance of 4 μF/cm^2, a barrier resistance of 10 Ω × cm^2, and a specific resistance of the medium of 54 Ω × cm. The impact of cell−substrate distance is illustrated in Figure 1B. As expected, the impedance (|Z|) measured at a fixed frequency of 4 kHz decreases with increasing cleft size. Hence, detachment of cells due to dissolution of focal contacts should result in a decrease of impedance. However, concomitant dissolution of cell−cell contacts would also result in an impedance decrease and are only discernible from spectral sweeps.

Quartz Crystal Microbalance (QCM). The QCM is based on thin disks made from α-quartz that are sandwiched between two metal electrodes. Because of the piezoelectric nature of α-quartz, any mechanical deformation of the crystal creates an electrical potential difference at the quartz surfaces and vice versa. Thus, mechanical oscillations of the crystal can be triggered and recorded electrically. For microgravimetry, solely AT-cut resonators are used that allow exciting shear oscillations parallel to the surface with the maximum amplitude at the center of the crystal faces (Thickness shear mode (TSM) resonator). At resonance, the resonator responds very sensitively to the adsorption of a foreign material on the electrodes. In principle, it is possible to measure the acoustic load of the resonator produced by the deposition of single- or multiple-component coatings such as fluids (Newtonian and Maxwellian), viscoelastic media, and rigid solids as well as combinations of them. Apart from measuring the complex impedance in the frequency regime of quartz resonance, it is also possible to measure the motional resistance using phase-lock oscillators or more frequently with the so-called QCM-D technique that permits one to record both the resonance frequency and the dissipation as a function of time ($U = U_0 \exp(-t \cdot \delta) \sin(2\pi ft + \varphi)$ with the dissipation $D = \delta/\pi f$).[35,36] Either technique allows one to measure the viscoelastic properties of foreign loading. Importantly, the so-called Sauerbrey relationship, which predicts a linear relationship between frequency change and deposited mass, therefore the term *microbalance*, does not hold for cells attached to the quartz crystal.[37] The cell bodies do not behave like a rigid mass layer but much more like a viscoelastic body. Thus, it is generally not valid to translate the observed frequency shift to biomass simply using Sauerbrey's equation and the integral mass sensitivity of the device. Ignoring this fact and applying the Sauerbrey relationship anyway leads to a significant underestimation of the cell mass by QCM measurements.[38]

Bandey et al. developed a general model that describes the electrical response of TSM resonators subject to a variety of load conditions also encompassing multilayer systems.[39] The most general case, nonlinear multiple loading, provides a mechanical impedance Z_s that allows one to model the impact of thin homogeneous films on top of the quartz surface. Changes in frequency and dissipation can be conversely related to changes in thickness, density, as well as storage (G') and loss modules (G''). Scheme 1 shows how we envision the acoustic load imposed by a cellular monolayer. Notably, the multilayer model holds strictly only for homogeneous layers.

The next section investigates how the parameters obtained from QCM measurements (f, δ) mirror mechanical and dynamical aspects of cell monolayers in contact with the resonator's surface. Figures 2A,B illustrate the influence of cellular height of the monolayer and cell−substrate distance on frequency and dissipation shifts measured by QCM in dissipation mode (D-QCM) employing an acoustic multilayer-model introduced by Bandey et al.[39] The three layer acoustic model consists of a thin layer (thickness h_{fl}) of aqueous media assuming a density of ρ_{fl} = 0.997 g/L and a viscosity of (η_{fl} = 0.89 × 10^{-4} Pa × s) followed by a viscoelastic layer representing the confluent cell monolayer exhibiting a finite thickness (h_c) and a complex shear modulus (G' = 50 kPa, G'' = 100 kPa) which is in contact with a semi-infinite aqueous layer on top of the cells (ρ_{fl} = 0.997 g/L and η_{fl} = 0.89 × 10^{-4} Pa × s). We assume that the layers of the composite system are connected in a nonlinear fashion. From extrapolation of microrheology data (not shown) assuming a power law dependence of the storage modulus $G' \sim f^{0.28}$ and Newtonian behavior of the loss modulus $G'' \sim \eta\omega$, we arrive approximately at a storage modulus of 30−60 kPa and a loss modulus 40−100 kPa at 5 MHz for MDCK II cells.[40]

While an increase of the water layer between the cells and substrate leads to a linear decrease in acoustic load (decrease of frequency and dissipation shifts), the impact of cell height is more pronounced and less straightforward due to the viscoelastic nature of the cell monolayer (Figure 2A,B). The frequency shift as a function of cell height resembles the time course found for cellular adhesion and growth to confluence.[31] Although the overall response of the quartz resonator is influenced by

Scheme 1[a]

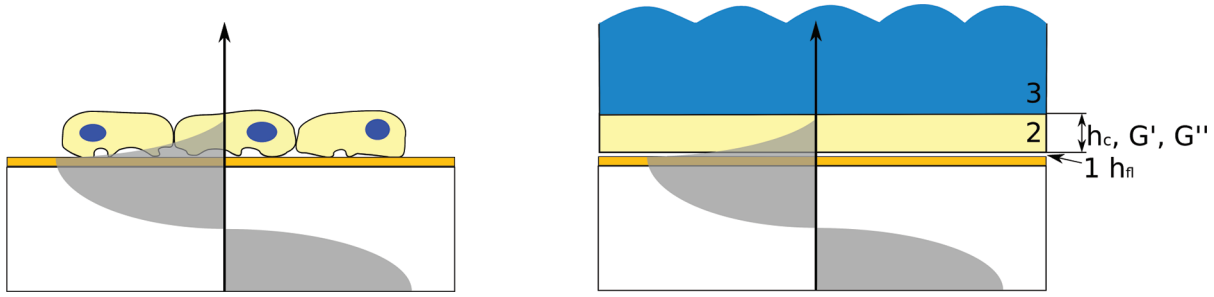

[a] (Left) Quartz crystal coated with a cell monlayer exhibiting a defined height h_c, cell−substrate distance h_{fl}, density ρ_c, storage modulus G', and loss modulus G''. The cells are in contact with a semi-infinite layer representing a Newtonian fluid with viscosity η_{fl} and density ρ_{fl}. (Right) Multilayer model capturing the essential features of A.

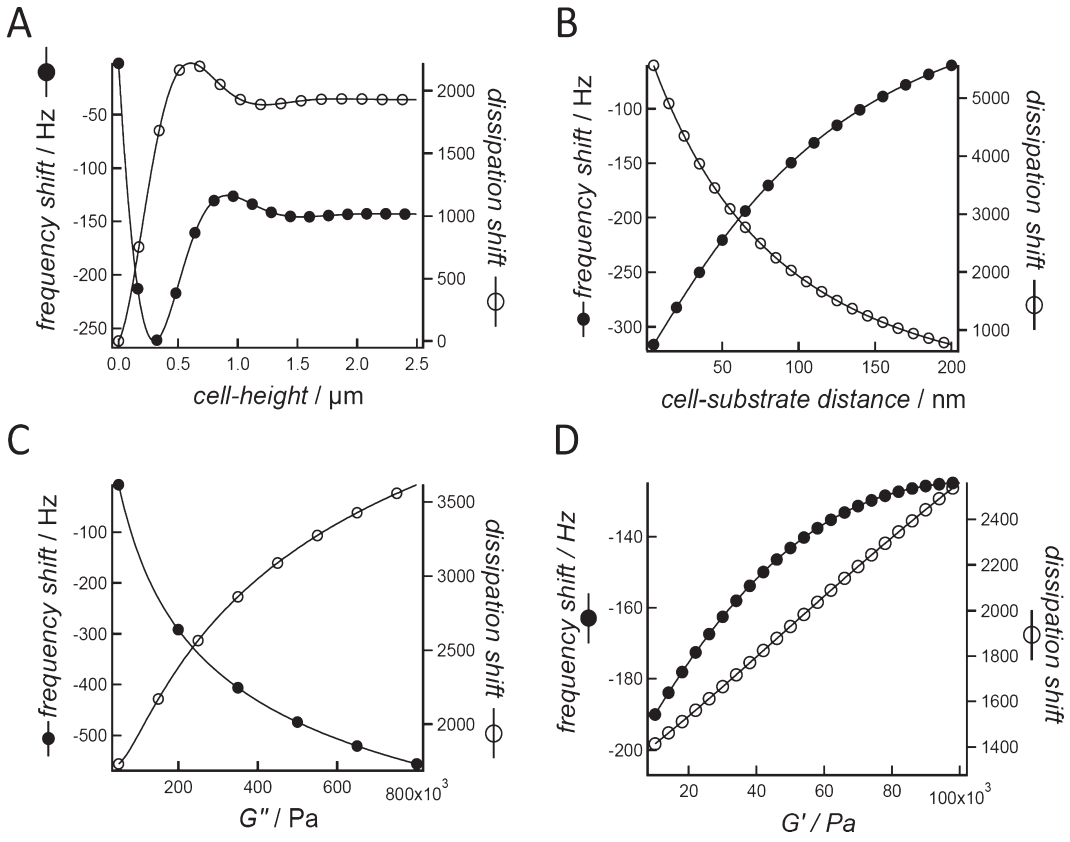

Figure 2. (A) Computed frequency and dissipation shifts depending on the height of the cellular monolayer assuming a three layer acoustic model in contact with a 5 MHz thickness shear mode resonator. (B) Calculated changes in resonance frequency and dissipation as a function of cell−substrate distance. (C,D) Change of frequency and dissipation as a function of the storage modulus (G') and loss modulus (G'') assuming a thin viscoelastic cell layer (h_c = 6 μm) covered with water.

electrode coverage with cells and their viscoelastic properties, it is conceivable that erection of the cells to form a confluent monolayer might be partly reflected in the observed frequency change. The response of the thickness shear mode resonator becomes substantially more intricate if the modulus (G') and loss modulus (G'') of the cell monolayer are varied (Figure 2C,D).

In fact, an increase in G' might lead to an increase in frequency *and* dissipation, while an increase in cellular viscosity leads to a shift to lower resonance frequency and larger dissipation.

This has one important consequence for the response of cells to the addition of toxins acting on both the cell−substrate distance and the elastic modulus of the adherent cells. While an increase in frequency should be expected for cells detaching from the surface (Figure 2B), a softening of the cells might lead to a frequency decrease (Figure 2C). Notably, the operational distance of the shear wave penetrating into the cell monolayer with the aforementioned morphology and elasticity decays within 1−2 μm (Figure 2A) rendering this method insensitive toward change on the apical side of the cell monolayer.

In conclusion, the deviation from a purely gravimetric behavior of the resonator as predicted by Sauerbrey for thin stiff adlayers is obvious for glassy or rubbery behavior of the cells. Changes in the viscoelastic properties of cells as a function of external stimuli lead to an intricate

dx.doi.org/10.1021/tx200115q |*Chem. Res. Toxicol.* 2011, 24, 1494–1506

Scheme 2. Chemical Structures of the Small Molecule Inhibitors Applied to Confluent Cell-Monolayers Used in the Present Study[a]

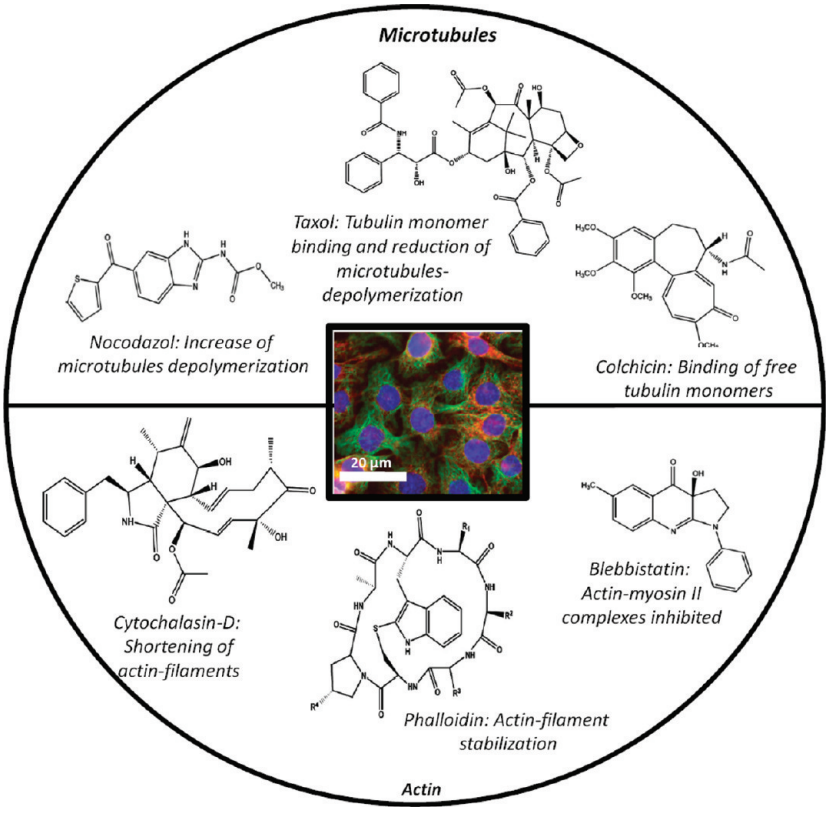

[a] Compounds that manipulate actin filaments are cytochalasin D (Cyt.D), phalloidin (Phall.), and blebbistatin (Blebb.); agents interfering with microtubules are paclitaxel, nocodazol, and colchicin; The center shows FaDu cells stained with Alexa Fluor 546 phalloidin for f-actin (red) and Alexa Fluor-488-conjugated IgG1 anti-β-tubulin for microtubules (green) and nuclei (blue) using 4′,6 diamidino-2-phenyindole (DAPI).

response of the resonator, which comprises shifts in resonance frequency to lower or higher values.

Fluctuation Analysis. The time series obtained from either QCM (Δf and $\Delta\delta$) or ECIS ($\Delta U_{in\text{-}phase}$) measurements were divided into blocks of 500 points (with an overlap of 50% between single blocks for F-QCM) and linearly detrended to remove long-term (thermal) drifts and offsets. Fast Fourier transformation (FFT) was carried out to gain power density spectra (PSD). The slope m of the PSD was determined by linear least-squares fits between 0.03 and 0.01 Hz for ECIS and 0.5−5 mHz for F-QCM. Long-memory dependence or persistence in time series is generally associated with power-law correlations, which means a larger slope m corresponds to higher time correlation, i.e., long-memory.[14]

RESULTS

The aim of this study was to investigate the suitability of acoustic and electric sensors to monitor the impact of toxins (Scheme 2) that alter the cytoskeleton organization of eukaryotic cells in a predictable manner for reliable use as noninvasive whole-cell biosensors. Apart from changes of the acoustic load (D-QCM) and electrical impedance (ECIS) as a function of time and dose, we also focus on the question whether or to what extent dynamic parameters derived from noise analysis generate a more sensitive and selective response as compared to the conventional readout and classical biochemical assays.

For this purpose, the impact of the various toxins on both, the noise amplitude, i.e., variance, and the long-term correlation obtained from the slope of the power density spectrum was measured and correlated with the specific role of the cytoskeletal components. Two different cell lines, a human squamous cancer cell line (FaDu) and a mammalian kidney cell line (MDCK II), were used in comparison. The focus of this study, however, lies on the impact of toxins acting on the cancerous cell line (FaDu). The corresponding data concerning MDCK II cells can be largely found in the Supporting Information. Scheme 2 gives an overview of the specific cellular effects of each inhibitor used in this study. The image in the center shows FaDu cells stained to visualize the actin cytoskeleton (red), microtubules (green), and the nucleus (blue).

IC_{50} Values of Small Molecule Inhibitors. As a first approach to determine the effective concentration regimes of the toxins under investigation and to set an established standard, MTS tests were carried out to determine the IC_{50} values for all six agents (Scheme 2), subdivided into two categories: (i) actin-related reagents such as cytochalasin D, phalloidin, and blebbistatin and (ii) microtubules altering substances like paclitaxel, nocodazol, or colchicin.

Differences between the two cell lines such as the expression of cytoskeletal components, the metastatic potential, and therefore cytoskeletal dynamics as well as membrane permeability issues produced IC_{50} values within a wide concentration regime. Table 1 and Table 1S (Supporting Information) summarize the results of the MTS tests for the two cell lines. Phalloidin is

generally less toxic than cytochalasin D, while an increase of the metabolism of FaDu cells under the influence of blebbistatin was found, possibly due to a synthesis overshoot as a response to its ATPase inhibiting activity. Equitoxic IC_{50} regimes for all chemicals applied in this study are summarized in Table 1.

Morphology of FaDu cells. Optical microscopy images of FaDu cell monolayers taken 24 h after seeding to confluence are shown in Figure S1 (Supporting Information). Occludin (1) and ZO-1 (2) fluorescence of FaDu cells is not cell-border located. The corresponding phase contrast image (3) supports the incomplete tight-junction formation of the cancer cell line by showing variable intercellular spacing. In contrast, MDCK II cells express pronounced barrier properties as revealed by ZO-1 staining (Figure S1, Supporting Information) and a considerable barrier resistance (>60 Ωcm^2).

Influence of Toxins on Cellular Impedance, Cell−Cell Contact Density, and Cell−Substrate Dynamics. The cellular response to toxins is monitored by ECIS and D-QCM providing a large variety of different parameters related to dynamic morphological and viscoelastic changes of the cells in response to the various external chemical stimuli. The oscillating quartz resonator is capable of detecting subtle changes in viscoelasticity due to an evanescent shear wave penetrating through the basal membrane of cells. Impedance spectroscopy captures adhesion and spreading of cells as well as temporal cell shape changes and cell−cell or cell−substrate dynamics. For the sake of clarity, we will exemplarily show only the raw data obtained from ECIS and QCM analysis for two different toxins. A representative set of kinetic data for all substances is shown in Figure S2 (Supporting Information). In order to keep information concise, we compiled all data represented by key parameters into single plots (vide infra).

Table 1. Average IC_{50} Values of All Toxins Acting on Actin or Microtubules for the Human Squamous Carcinoma Cell Line FaDu Derived from the Hypopharynx[a]

toxin	IC_{50} FaDu/μM
cytochalasin D	30
phalloidin	970
blebbistatin	730
colchicin	745
nocodazol	50
paclitaxel	145

[a] The means of three experiments with each $n = 6$ and SD of ±15% are given.

Figure 3A exemplarily shows a typical set of kinetic data obtained from ECIS-measurements of FaDu cells exposed to cytochalasin D (Cyt.D). $|Z|_{norm}$(4 kHz), as well as the two fluctuation related parameters, the slope of the PSD m^{PSD}_{ECIS}, and the normalized variance $\tilde{\sigma}^2_{ECIS}$ are shown. Untreated cells are displayed in green and empty electrodes in black. The orange lines represent the response of cells to the addition of cytochalasin D at IC_{50}. The time course of the experiment can be deliberately divided into five regimes: subconfluent stage (a), confluence (b), time of adding the toxins (c), and 0−24 h interval (d), interval from 24 h to the end of the experiment, lasting usually 72 h (e). The gray-shaded area (a,b) corresponds to the time before the addition of the toxin, flanked by the time interval representing the addition of the toxin (c).

The time period (c) was excluded from noise evaluation due to the inevitable thermal perturbation of the system produced by the addition of compounds to the culture medium. $|Z|_{norm}$, m^{PSD}_{ECIS}, and $\tilde{\sigma}^2_{ECIS}$ were normalized to mean value of time interval b and standardized to the corresponding starting values obtained from

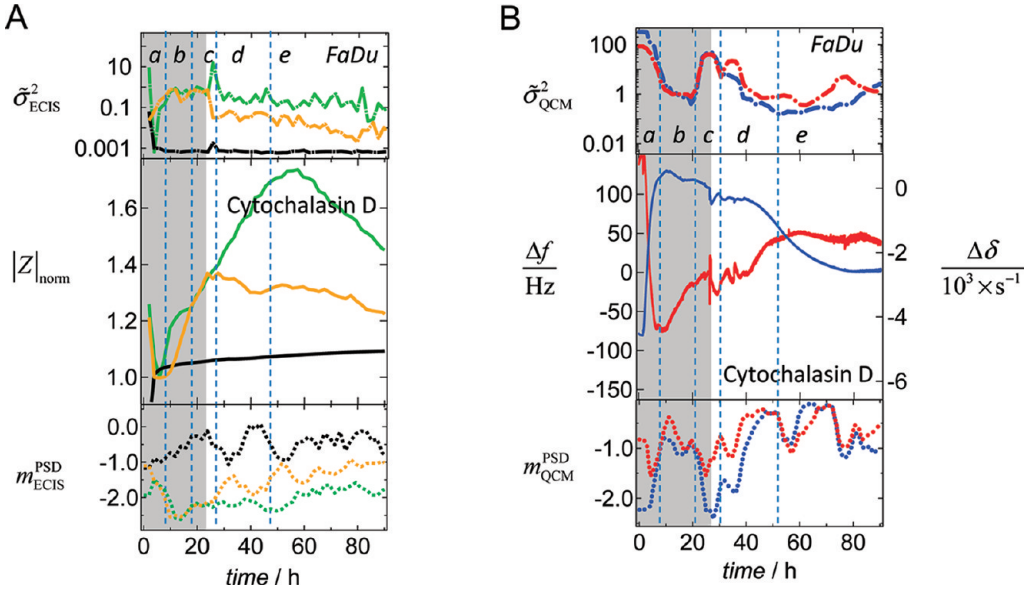

Figure 3. Kinetic change of a set of parameters obtained from electric cell−substrate impedance sensing (ECIS)-measurements (A) and Quartz crystal microbalance with dissipation monitoring (D-QCM) (B), after an exposure of the 6×10^5 FaDu cell inoculum to cytochalasin D. The time interval prior to the addition of cytochalasin D (30 μM) is marked in gray. From top to bottom: variance $\tilde{\sigma}^2_{ECIS}$ or $\tilde{\sigma}^2_{QCM}$ (normalized to variance of confluent cells), magnitude of complex cellular impedance $|Z|_{norm}$ (after cytochalasin D treatment (orange), untreated cell monolayer (green), and electrode immersed in full culture medium without cells (black), normalized to the starting value, recorded at 4 kHz, and frequency and dissipation shifts Δf (red) and $\Delta\delta$ (blue) (both normalized to toxin addition) and PSD-slopes m^{PSD}_{ECIS} or m^{PSD}_{QCM}, respectively. Five consecutive time regimes are distinguished: seeding/spreading and polarization (a), confluency (b), toxin addition (c), 0−24 h interval, and >24 h interval until the end of experiment (e).

dx.doi.org/10.1021/tx200115q |Chem. Res. Toxicol. 2011, 24, 1494–1506

a. All measurements were carried out at least in triplicate showing the same general trend.

Addition of cytochalasin D reduced the impedance $|Z|_{norm}$ and the slope of the PSD as well as the variance. We attribute the general increase in $|Z|_{norm}$ of untreated cells to their growth (time intervals c,d,e), proliferation, and spreading. Exposure to cytochalasin D reverses this trend. Around 60 h after the seeding of the cells, the control displays a decreasing impedance $|Z|_{norm}$ accompanied by a declining slope of the PSD and noise amplitude (variance).

Biological Activity of Cells Cultured on Thickness Shear Mode Resonators. Figure 3B shows the response of FaDu cells exposed to cytochalasin D (at IC_{50}) employing F-QCM readouts. The F-QCM monitors fluctuations of resonance frequency changes Δf and dissipation changes $\Delta\delta$ as a function of external stimuli and hence delivers information about cellular dynamics, i.e., shape and viscoelastic fluctuations. The fluctuations are characterized by m^{PSD}_{QCM}, the slope of the PSD and $\tilde{\sigma}^2_{QCM}$, and the variance of both f and δ. In contrary to the micromotion measured by ECIS, no information on the integrity of cell−cell contacts can be directly inferred.

We arbitrarily set both frequency and dissipation to zero upon addition of toxins. On average, seeding of FaDu cells shows overall Δf-shifts of $-(205 \pm 35)$ Hz and $\Delta\delta$-shifts of (5080 ± 110) s^{-1}. F-QCM fluctuation analysis of the PSD obtained from resonance frequency noise of the cell covered TSM resonators produces mean PSD slopes of −0.9 indicative of biological activity.[16]

Upon the addition of cytochalasin D, frequency (Δf) and dissipation ($\Delta\delta$) shifts show a trend in the opposite direction for both cell lines, while f increases, and δ decreases. Both parameters eventually reach a plateau by the end of the experiments, indicative of the partial loss of attached viscoelastic load close to the cell-free level. This can be interpreted in terms of cells lifting up from the electrode, thus increasing the cleft between cells and the substrate h_{fl} (Figure 2). Untreated cells in contact with the resonator monitored over the same time interval essentially revealed unchanged viscoelasticity and cell−substrate distance of the epithelial cell layers as well as constant fluctuation parameters. The toxin evokes both, reduced fluctuation amplitudes, as inferred from a reduction of $\tilde{\sigma}^2_{QCM}$ (f and δ) after the addition of cytochalasin D at IC_{50} concentration, and it reduces the long-term correlations captured by m^{PSD}_{QCM} of f and δ.

The influence of cytochalasin D on cellular dynamics (m^{PSD},$\tilde{\sigma}^2$) generated by adherent cells becomes apparent in the first 24 h of exposure. For MDCK II cells both positive as well as negative frequency shifts toward lower resonance frequency are frequently observed depending on whether cell detachment or softening of cells dominates the response (Supporting Information).

Correlation of Sensor Output with Cytoskeleton Organization. *Resonance Frequency f, Dissipation δ, and Overall Impedance |Z|.* Figure 4 summarizes the impact of toxins either interfering with the organization and dynamics of the actin cytoskeleton (top) or influencing microtubule organization (bottom) on the acoustic and impedimetric parameters Δf, $\Delta\delta$, and $\Delta|Z|_{norm}$, respectively. We refer to these parameters as stationary ones to distinguish them from their dynamic counterpart derived from noise analysis. Generally, results from D-QCM (Figure 4A) and ECIS measurements (Figure 4B) show a similar trend, while D-QCM parameters (Δf, $\Delta\delta$) respond less sensitively to cell specific toxins than the ECIS parameter $|Z|_{norm}$.

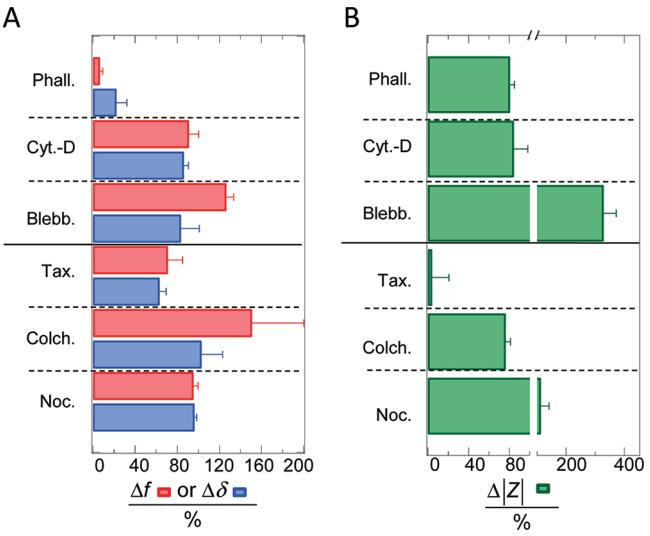

Figure 4. Comparison of D-QCM (A) and ECIS (B) sensor responses to equitoxic, IC_{50}-concentrations of small molecule inhibitors (actin and microtubules agents). The direct readout parameters of D-QCM (Δf and $\Delta\delta$) and ECIS ($|Z|_{norm}$) are shown for FaDu cells. 100% refers to cells before treatment and 0% to the cell free electrodes. Values are averaged over 24 h after exposure to toxins at IC_{50}. Note the split axis for B.

Notably, the response of the cell covered sensors is more diverse and selective than conventional biochemical tests which almost exclusively show a decrease in vitality. These tests, however, do not capture changes in cellular stiffness or the distance of cells from the substrate.

In the following section, we describe how the various agents interfere with cytoskeleton organization as derived from stationary parameters. The corresponding data for MDCK II cells can be found in Supporting Information.

Actin Agents. The actin stabilizing phalloidin causes a considerable impact on D-QCM parameters (Δf, $\Delta\delta$) of FaDu cells displaying a reduction of 60% (increase in f and decrease in δ), while $|Z|_{norm}$ is only slightly reduced (to 80%). Along the lines, addition of actin-destabilizing cytochalasin D to FaDu monolayers also produces a decrease of $|Z|_{norm}$ by 20% corresponding to untreated cells, while both f and δ remain largely unchanged. Blebbistatin produces a strong increase in cellular impedance, while D-QCM parameters are generally less affected.

Microtubules Agents. Small molecules affecting microtubules show generally a stronger sensor response upon stabilization than destabilization. Paclitaxel, known to stabilize microtubules, strongly reduces $|Z|_{norm}$ (below 10%), while the QCM parameters δ and f are reduced by 20%. Colchicin, which binds free tubulin monomers, does not impact δ but produces an increase in f to 130%. In turn, colchicin causes a slight decrease of $|Z|_{norm}$ to 80%.

FaDu cells treated with nocodazol, which increases microtubule depolymerization, however, display neither a QCM response nor an ECIS response.

Generally, FaDu cells display a typical response to the addition of toxins that is best explained by the loss of cell−substrate interaction giving rise to a decrease in impedance and increase in resonance frequency accompanied by a decrease in energy dissipation in comparison to vital untreated cells. MDCK II cells (Supporting Information), however, often show a decrease of f and δ as a response to toxin exposure, which is indicative

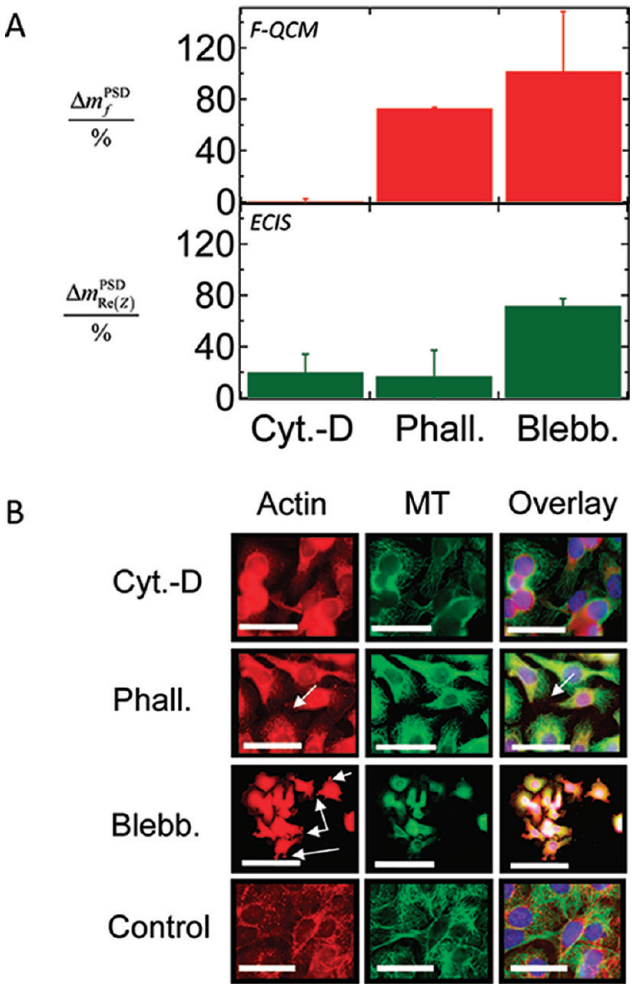

Figure 5. (A) Cellular dynamics altered by actin manipulating agents such as cytochalasin D (Cyt.D), phalloidin (Phall.), and blebbistatin (Blebb.) added at their corresponding equitoxic IC_{50} (Table 1). Biological noise originating from fluctuations in frequency f and cellular impedance are analyzed in terms of PSD-estimation resulting in time-dependent slopes $m^{PSD}_{QCM/ECIS}$ monitored in the interval from 24 to 72 h. Standardization to percentage data is achieved through the corresponding values at confluence (time regime (b), 100%) and the empty electrode signal (starting values of time regime (a), 0%); $m^{PSD}_{QCM/ECIS}$ describes long time correlations in cellular fluctuations. (B) Fluorescence micrographs visualize cell specific small molecule effects on cytoskeletal integrity of FaDu cells by Alexa Fluor 546 phalloidin f-Actin staining (red), Alexa Fluor-488-conjugated IgG1 anti-β-tubulin labeling (green), or DAPI-dye for the visualization of nucleus localization in overlays. The corresponding controls of untreated cells are given in the last row. Scale bars correspond to 125 μm in the Blebbistatin images and 50 μm otherwise.

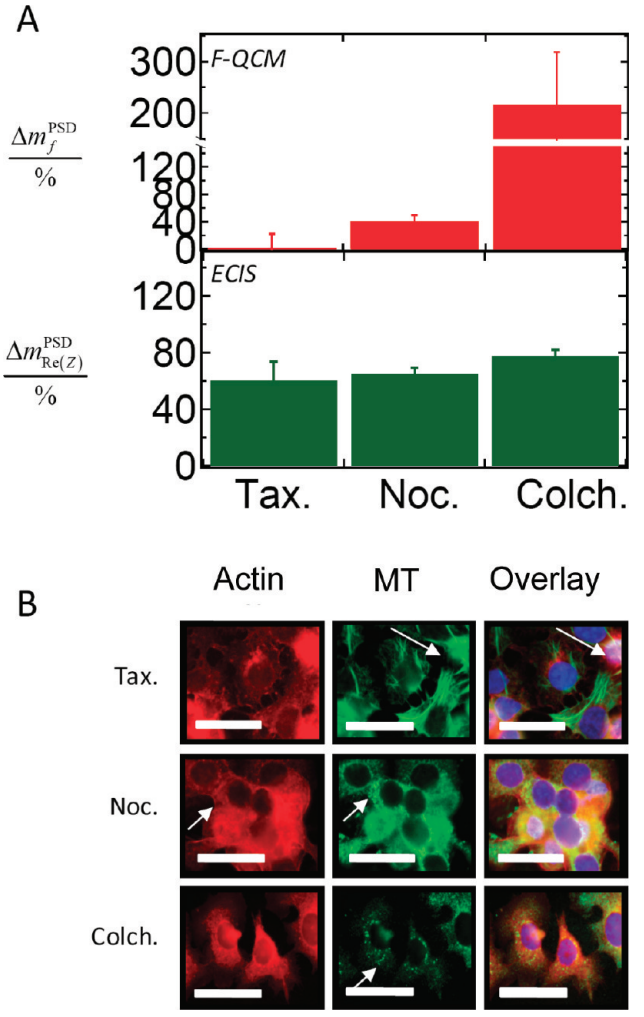

Figure 6. (A) Alteration of cellular dynamics by the addition of small molecule inhibitors that are directed to microtubule organization corresponding to the 24−72 h interval: paclitaxel (Tax.), nocodazol (Noc.), and colchicin (Colch.) added at their corresponding IC_{50}. (B) Fluorescence micrographs display cell specific small molecule effects on the cytoskeleton integrity of FaDu cells employing Alexa Fluor 546 phalloidin f-Actin staining (red), Alexa Fluor-488-conjugated IgG1 anti-β-tubulin labeling (green), and DAPI-dye (blue) for visualization of nucleus localization in overlays. The corresponding controls of untreated cells are given in the last row of Figure 5B. The scale bar of each image corresponds to 50 μm.

of cell-softening (Figure 2). Tables compiling all relevant parameters for both cell lines are given in the Supporting Information (Tables S1−S3).

Shape and Viscoelastic Fluctuations Measured by ECIS and F-QCM PSD Estimation. ***Actin Agents.*** In Figure 5A, the effects of cytochalasin D, phalloidin, and blebbistatin on the noise parameters m^{PSD} of f (F-QCM) and $|Z|_{norm}$ (ECIS), respectively, are shown. Figure 5B allows one to correlate noise parameters to cell-specific effects of the toxins on the cytoskeleton architecture deduced from fluorescence microscopy. Micrographs depict phalloidin-stained actin in red, anti-β-tubulin-labeled microtubules in green, and the overlay including DAPI-stained nuclei (blue) for facilitation of intracellular localization.

Within the time interval (24−72 h), the actin-destabilizing and -shortening effect of cytochalasin D is reflected in a significant reduction of all parameters describing the fluctuation of acoustic and electric impedance (see also Table S2, Supporting Information).

ECIS micromotion responds more moderately to the exposure of toxins than F-QCM. Microscopically (Figure 5B), a clearly disrupted actin cytoskeleton is visible lacking stress fibers and a cortical ring, while the cells show actin aggregates/plaques in nuclear vicinity as a consequence of actin depolymerization.

Noise parameters such as variance and PSD slope are also impacted by the actin-stabilizing effect of phalloidin. The

dx.doi.org/10.1021/tx200115q |*Chem. Res. Toxicol.* 2011, 24, 1494–1506

m_{QCM}^{PSD} of FaDu cells remains at 75%, while micromotion analysis of ECIS data (m_{ECIS}^{PSD}) turned out to be more responsive to phalloidin than F-QCM data dropping below 25%.

Fluorescence micrographs (Figure 5B) display long, stiff actin fibers associated with a large amount of substrate contacts (see the fibers and dots marked by arrows). FaDu cells exhibit no significant shape changes upon toxin treatment, possibly explaining the small decrease of m_{QCM}^{PSD} found for the latter cell type.

Blebbistatin, which blocks actin−myosin II ATPase in the actin-unbound state, increases m_{QCM}^{PSD} by 10−25% (Figure 5A). However, impedance noise parameters m_{ECIS}^{PSD} are diminished by 30% for FaDu cells. The corresponding fluorescence micrographs show a dense actin cytoskeleton but elongated cell bodies with filopodia-like extensions (see arrows in Figure 5B, third row). The altered monolayer architecture might be responsible for the observed change in collective vertical motility (vide infra).

Microtubule Agents. In Figure 6, the impact of toxins interfering with microtubule organization on the biological noise mirrored in the slope of the power density spectrum taken from the fluctuations in resonance frequency of the QCM and impedance fluctuations is shown. Generally, paclitaxel (Figure 6A) reduces the overall noise and correlation time regardless of cell type and sensor (see also Tables S1 and S2, Supporting Information). Both cell types display a considerable reduction of all noise parameters derived from F-QCM and ECIS micromotion. Figure 6B (upper row) visualizes the impact of paclitaxel on microtubule organization: FaDu cells show strong aggregation of microtubules into bundles (arrow in green channel), whereas the actin skeleton of both cell lines remains fairly unaffected (Figure 5B, lower row).

Addition of nocodazol to FaDu cells results in a significant reduction of m_{QCM}^{PSD} and m_{ECIS}^{PSD} (Figure 6A). Fluorescence micrographs (Figure 6 B, middle row) reveal a strong degradation of microtubules. The actin network shows slight reorganization upon microtubule degradation (arrows in red and green channel of micrographs from nocodazol treated FaDu cells).

Remarkably, we find a substantial increase of m_{QCM}^{PSD} values for FaDu after the addition of colchicin at IC_{50}. In contrast, the corresponding change in micromotion measured by ECIS shows only a slightly reduced PSD slope. When compared to micrographs (Figure 6B, lower row), we find a slight reorganization of the actin cytoskeleton (red channel arrow) upon microtubule degradation. The accompanying reorganization of the actin filaments might be responsible for this selective sensor response. For all small molecule inhibitors presented above, PSD estimation was also performed for fluctuation of the dissipation signal (Table S1, Supporting Information). Apart from blebbistatin and nocodazol added to MDCK II cells, all other experiments revealed a decrease in the PSD slope for fluctuations of δ corresponding to a loss of vitality. Additionally, variance frequency, dissipation, and impedance time courses are summarized in Table S2 (Supporting Information).

DISCUSSION

In the present study, we investigated the impact of a variety of small molecule inhibitors of the main intracellular locomotive machinery encompassing actin fibers, microtubules, and the motor protein myosin II on the electric impedance and acoustic load of two epithelial cell lines MDCK II and FaDu. The basic idea of this study is to elucidate to which extent parameters derived from electrical and acoustic sensors are suitable reporters for cell viability. While biochemical cytotoxicity tests such as MTS, MTT, or LDH basically report on the general viability of cells, acoustic as well as impedimetric biosensors such as QCM or ECIS are noninvasive, label-free, and detect biological activity from an electrical *and* mechanical viewpoint. Here, we scrutinize the aptitude of the two methods to substitute or complement existing biochemical cytotoxicity assays for detecting toxins acting on the cytoskeleton. In an attempt to assign biological or cellular observables to the measured parameters using ECIS and QCM, we carried out computations of the sensors' responses as a function of cell−substrate distance, height of the cell monolayer, and viscoelastic parameters (Figure 2). Generally, the across-the-board statement that impedance decreases due to larger cell−substrate distance and loss of barrier properties, while the resonance frequency of the TSM resonator increases due to the loss of acoustic load as a response to addition of toxins could be reproduced. However, some subtleties require our attention. For instance, it is conceivable that cells become softer and at the same time detach slightly from the substrate as a response to actin severing agents. In this case, the overall response of the quartz resonator is difficult to predict since softening might lead to an increase in the negative resonance frequency shift toward a lower resonance frequency, while lifting of the cells from the electrodes generates a change in the opposite direction (vide supra). A concomitant increase in both resonance frequency and dissipation is a good indication that indeed cells became softer after toxin treatment (Figure 2C). If, however, dissipation and frequency shifts show opposite trends, for instance increase in resonance frequency and decrease of dissipation, cell detachment or increase of the cell−substrate distance might be responsible. Notably, changes in impedance and resonance frequency are only indirect measures of cell−substrate distance. In contrast, if the resonance frequency decreases and dissipation increases a closer contact of the cells to the gold electrode on top of the quartz crystal might be inferred. As a consequence, it is important to compare $\Delta f-\Delta\delta$ trends after exposure to the corresponding toxin in order to judge whether cell detachment might prevail over softening.

In general, we can divide our measurements into those which rely on the observables that are linked to the sensor readout such as impedance of the gold electrode as a function of frequency or resonance frequency of the quartz crystal and those which are generated from the fluctuations of the observables. As a consequence, we refer to stationary parameters for the former set of parameters, while dynamic parameters represent the latter ones. Stationary parameters comprise the cellular impedance $|Z|_{norm}$, obtained at a fixed frequency (4 kHz), the mass change represented by the shift in resonance frequency (Δf), and the change in viscoelasticity ($\Delta\delta$) derived from damping of the quartz crystal, while dynamic parameters are derived from fluctuations in impedance (ECIS) and resonance frequency (F-QCM) such as slope of the power spectra density m generated from the fluctuations of impedance or resonance frequency.

Figure 7 summarizes the findings of the present study by merging the effect of the drugs stalling the polymerization of actin (red↓) or microtubules (green↓) and drugs that abolish depolymerization (↑). All values are either taken 24 h (continuous lines) or 72 h (dotted lines, only shown for dynamic parameters) after exposure of the cells to the respective drug. The concentration of the respective drug was chosen corresponding to the IC_{50} as determined by prior MTS tests. The four diagrams compile the average data found for the two cell lines FaDu and MDCK II and

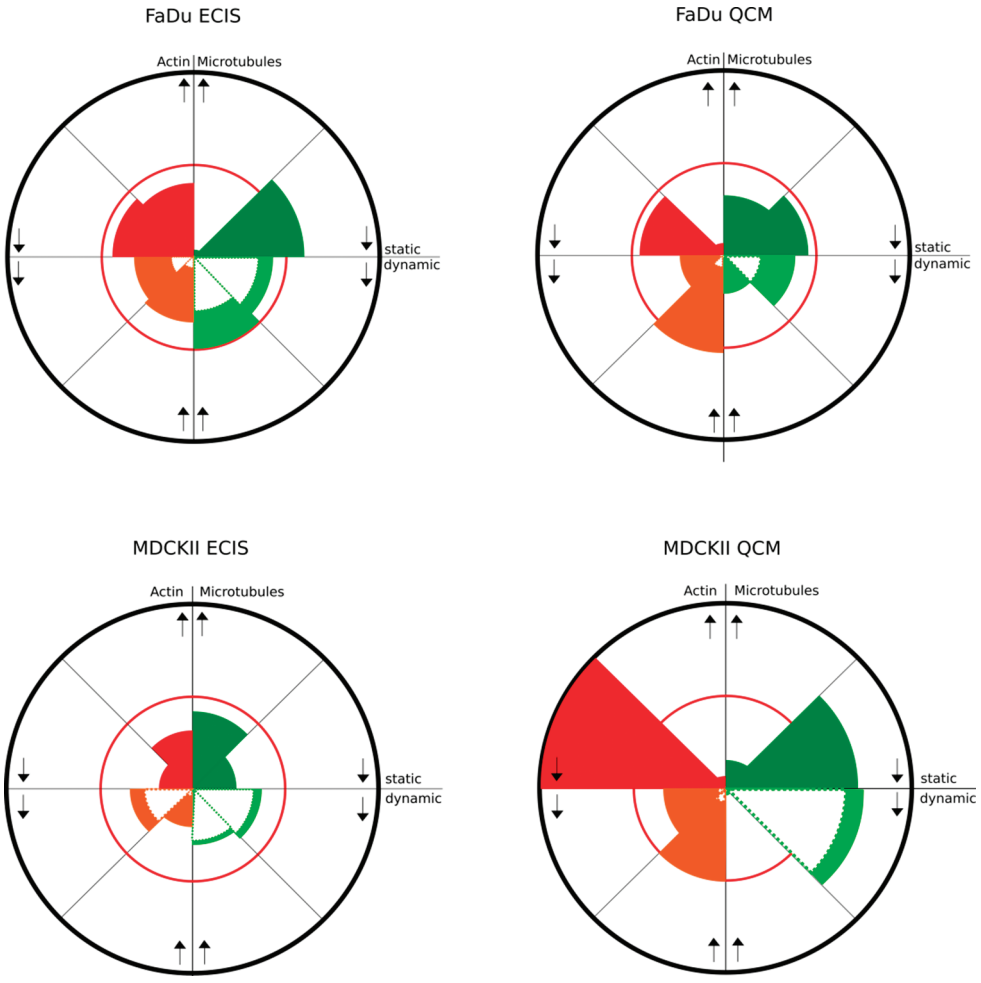

Figure 7. Pie charts illustrating the effect of various drugs on static (i.e., Δf and $\Delta|Z|_{\mathrm{norm}}$, top half) and dynamic (i.e., $m_{\mathrm{QCM}}^{\mathrm{PSD}}$ and $m_{\mathrm{ECIS}}^{\mathrm{PSD}}$, bottom half) parameters derived from F-QCM and ECIS measurements. The color code assigns red and orange to drugs acting on actin filaments and dark/light green to drugs perturbing microtubule organization. Arrows represent the specific action (stabilization/destabilization) of the drug on the biopolymer: ↑ refers to phalloidin (actin) or paclitaxel (microtubules) and ↓ to cytochalasin D (actin) or nocodazol (microtubules). For better visibility, the values are normalized to the radius and not to the area. The red line corresponds to 100% vitality, i.e., untreated cells. The values after 24 h of exposure are represented by continuous lines, while those obtained after 72 h exposure time are shown framed in dotted lines (only given for the dynamic parameters).

the two sensors F-QCM and ECIS, respectively. The upper half of the pie charts display the so-called stationary parameters, in this case for the sake of simplicity only the change in Δf (QCM) and $|Z|_{4\mathrm{kHz}}$ (ECIS), while the bottom half shows the slope of the PSD spectra, $m_{\mathrm{QCM}}^{\mathrm{PSD}}$ and $m_{\mathrm{ECIS}}^{\mathrm{PSD}}$, respectively. The radius of the red circle represents 100% vitality corresponding to the values measured for untreated cells.

Impact on Static Parameters. Generally, we found that both cell lines respond to the exposure of drugs affecting the cytoskeleton with a reduction of the impedance, which we attribute to either loss of cells, cell−cell contacts, cell-shape changes (rounding), or an increase in the cell−substrate distance (Figure 7). Therefore, this readout signal is very reliable but neither very sensitive nor selective. More selective but less predictable are data derived from QCM readouts. Changes in the resonance frequency of the acoustic resonator turned out to be less responsive to depolymerizing agents, while exposure of cells to substances that stall depolymerization affects the acoustic load represented by the frequency shift more significantly. From Figure 2, it is obvious that frequency and dissipation changes as well as impedance changes compile many cellular properties such as cell shape, cell−substrate distance, or cell−cell contacts and therefore reflect biological activity in a unique but also intricate way preventing an unequivocal assessment of drug toxicity. This is best illustrated by measuring the impact of cytochalasin D on cells cultured on TSM resonators. It is known that cytochalasin softens the cells due to the dissolution of the actin network and at the same time lifts them off from the substrate since focal adhesion plaques disassemble.[41] While a cell softening generates a shift to lower resonance frequencies, cell detachment acts in the opposite direction. As a consequence, the response of the acoustic sensor becomes unpredictable and is therefore not a suitable reporter for cell vitality per se.

Fluctuations, however, mirror cellular vitality in a more direct manner since biological noise originates mainly from the dynamics of minuscule cell-shape changes displaying long-term correlation that allow one to distinguish live from dead cells. Recently, we reported on the use of resonance frequency fluctuations to measure the cytotoxicity of gold nanoparticles and distinguish the metastatic potential of cells.[16,17] Here, we extend this statement to well-known drugs acting on cytoskeleton organization.

Impact on Dynamic Parameters. In general, dynamic parameters act more sensitively on the addition of drugs that alter the

dx.doi.org/10.1021/tx200115q |*Chem. Res. Toxicol.* 2011, 24, 1494–1506

cytoskeleton organization than the MTS test (Figure 7). Fluctuations encompass dynamic shape changes, changes of the distance between cells and the substrate, and viscoelastic changes generating corresponding time series of the sensor signal. The time series usually display long memory behavior indicative of living cells that display a temporal fractal dimension reflecting long correlation times.

Micromotion as determined by ECIS is reduced in all cases, albeit actin-affecting agents impair micromotion to a larger extent than the toxins acting on microtubules. In contrast, F-QCM analysis is strongly susceptive to both microtubule- and actin-affecting drugs. Viscoelastic or shape fluctuations are also reduced or decay entirely to the instrumental noise level except for the depolymerization of microtubules producing an enhancement of fluctuation amplitude.

The general outcome of this survey is the fact that cellular dynamics as displayed by micromotion or viscoelastic/shape fluctuations respond to changes of the cytoskeleton organization significantly more sensitively than the conventional MTS test. Albeit the correlation between cytotoxicity and micromotion is strong, the information content of ECIS and QCM measurements is more complex. In the following section, we want to discuss possible scenarios and how to interpret the data in more depth taking into account the known effects of the drugs.

Phalloidin, an actin stabilizing and polymerization-promoting agent with poor membrane permeability,[42] reduces both the shift in resonance frequency and energy dissipation. A concomitant change of both parameters in the opposite direction, i.e., an increase in resonance frequency and decrease of dissipation, is indicative of a reduced acoustic load or detachment of cells. Since both the apparent mass (frequency shift) and impedance decrease, we assume that either shape changes as seen in the micrograph or an increase in the cell−substrate distance occurs. An increased cleft between cells and the substrate, i.e., the gold electrode, would result in a diminished acoustic load mirrored in a decrease of frequency and dissipation shifts as compared to that of the untreated cells (Figure 2A). Cytochalasin D treatment also results in a decrease of energy loss of the cells on the resonator. Albeit this is the general trend found for FaDu cells, we frequently observed a frequency shift for MDCK II cells in response to cytochalasin D treatment to lower values depending on toxin concentration. For instance, we found an increase in resonance frequency upon the addition of cytochalasin D at low concentration (∼5−10 μM), while a decrease of f and δ was found for its IC_{50} (30 μM). We attribute this decrease in frequency to a softening of cells generating a further decrease of the quartz's resonance frequency which outdoes the impact of cell detachment which would otherwise increase the resonance frequency. A concomitant change of dissipation in the same direction and only a small change in impedance support this interpretation.

In good agreement with the general trend found for our cell lines particularly at low doses of cytochalasin D, a shift of Δf to larger values accompanied by a loss in dissipation indicative of cell detachment was described for A549 cells by Marxer et al.,[25] for MDCK II cells by Wegener et al., [20] and for 3T3/NRK fibroblasts by Rotsch et al.[41] Micrographs of FaDu cells show a slight shape contraction upon the administration of cytochalasin D, which is captured by decreasing impedance.

Exposure to blebbistatin, which represses myosin II-ATPase activity,[43] might result in a slight decrease of cell rigidity attributed to a decreasing actin cytoskeleton stiffness as measured by microrheology, AFM, and optical tweezers.[44−46] The effect might, however, be masked by accompanying changes of the cell−substrate distance leading to a cell-specific response. We found an increase in Δf for both FaDu and MDCK II cells indicative of cell softening. In optical micrographs, prolonged cell extensions are found, which also might imply a closer cell−substrate distance.

Microtubules are stabilized and prolonged by paclitaxel treatment and form asters and fibers/bundles in fluorescence micrographs, whereas actin remains largely unaffected, as originally described.[47] Minor desorption of FaDu and MDCK II cells was monitored at IC_{50}, probably contributing to a reduction of mass and dissipation levels, which was also found by Marx et al.[29] Though elasticity and viscosity were often described to be only slightly changed,[25,41,48] we do not confirm this trend for IC_{50} of paclitaxel, as energy dissipation decreases significantly, especially for MDCK II cells. We find, however, an increased amount of apoptotic cells in both cell lines coinciding with an impedance breakdown, especially for FaDu cells. Recently, this was also observed by Arndt et al.[49] for cycloheximid-triggered apoptosis.

Nocodazol and colchicin, the former a synthetic benzimidazol and the latter a plant alkaloid, both destabilize microtubules by binding the dimeric subunit and elicit a secondary, regulatory effect on overall migration.[50] We found colchicin to reduce the acoustic load produced by MDCK II cells and to slightly increase the load exerted by FaDu cells on the resonator, whereas a decrease of $|Z|_{norm}$ was observed for both cell types. These on first sight contradictory effects might be attributed to the interplay between the lifting of cells and softening. Micropipet aspiration experiments revealed a similarity between neutrophils and FaDu cells under colchicin treatment. An increase of actin polymerization accompanied by an increase in cell rigidity and viscosity was found.[51] Elasticity of fibroblasts, however, was not found to be altered upon colchicin treatment.[41] Nocodazol provokes a reduction of $|Z|$ by 40−60% for MDCK II cells and a frequency decrease, which we explain by a reduced barrier resistance accompanied by a softening of cells. FaDu cells generate the opposite response, an increase in impedance but a decrease of Δf to lower resonance frequency. This can be explained by increased cell spreading or the induction of peripheral actin polymerization, which is controversially discussed in the literature.[24,29,52] Alterations of cellular dynamics represented by fluctuations in vertical motility draw the following picture: generally, vertical motility of cells is substantially suppressed by interfering with cytoskeleton organization. As mentioned above, in many cases noise parameters display higher sensitivity than static viscoelastic and impedimetric parameters. The same holds for the MTS-test, as values frequently undercut 50%. Particularly, elimination of the cell's capability to disassemble microtubules suppresses cellular fluctuations to a large extent. The same was found for drugs which reduce F-actin. Actin-stabilizing phalloidin shows almost no impact on noise parameters, while cytochalasin D efficiently reduces detected noise as a result of actin depolymerization. Contrary, stabilizing microtubules by paclitaxel reduces the noise levels, whereas we find an increase of fluctuations with blebbistatin or colchicin. The former observation correlates to a vitality measured by the MTS-test, exceeding 100%. A preponderance of studies ascribes this effect to deregulated actin-severing and 50% reduced retrograde flow in lamellipodia and filopodia.[9,50]

Regional metastasis formation in head and neck squamous cell carcinoma may decrease the patient's survival to merely 50%.[53,54] Therefore, besides directed disruption of cytoskeleton dynamics or force generation, our aim was to detect cancer cell-specific migration modes with our setup. The comparison of MDCK II cells to the cancer line FaDu on an MTS basis revealed generally higher

IC_{50} values for all drugs except for nocodazol administration. We found, however, that nocodazol (as all microtubules agents) elicited neither influence on the viscoelasticity of FaDu cells nor on $\Delta|Z|_{norm}$, whereas nocodazol clearly reduced all responses associated with cellular micromotion. Colchicin and blebbistatin even increased viscoelastic fluctuations of FaDu cells but reduced impedimetric fluctuations. We found that not only paclitaxel but also cytochalasin D were both efficient in reducing FaDu micromotion.

CONCLUSIONS

In the present study, we could show that cellular dynamics as measured by micromotion and viscoelastic fluctuations is a suitable and sensitive indicator for cell viability. In contrast, changes in resonance frequency or dissipation intricately depend on cellular properties such as cell shape, cell−substrate distance, or cell−cell-contacts and are therefore not necessarily correlated with cell viability. Albeit the readout of electric impedance is generally a reliable indicator for cytotoxicity, it is not very selective and less responsive than the dynamic readouts that rely on fluctuation analysis.

We were able to identify actin polymerization as well as microtubule depolymerization as the main contributors to viscoelastic or impedimetric fluctuations as detected by the quartz crystal microbalance in fluctuation mode (F-QCM) or electric cell−substrate impedance (ECIS) sensors. Paclitaxel and cytochalasin D proved to be sufficiently powerful to reduce the micromotility of human head and neck tumor cell line FaDu acting as anticancer drugs.

Both acoustic and electric sensors are noninvasive and label-free offering time-dependent analysis over a wide concentration range requiring only a small amount of cells. Hence, we expect stochastic whole-cell sensors to become a versatile and potent alternative to conventional cytotoxicity assays, in particular, if quick and selective responses are needed, and the material is sparse.

ASSOCIATED CONTENT

Supporting Information. This material is available free of charge via the Internet at http://pubs.acs.org.

AUTHOR INFORMATION

Corresponding Author

*Phone: +49-551-3910633. E-mail: andreas.janshoff@chemie.uni-goettingen.de.

Funding Sources

Financial support was granted by the graduate school of excellence MAINZ and the DFG through SPP 1313 "Bionanoresponses" and the SFB 937 "Collective Behavior of Soft and Biological Matter".

ACKNOWLEDGMENT

We thank Analuisa Nava, Stefan Beulig, Dennis Manz, Stefanie Klassen, Anja Herdlitschke, Angela Rübeling, and Dr. Ingrid Schuberth for helpful discussions.

REFERENCES

(1) Woodhouse, E. C., Chuaqui, R. F., and Liotta, L. A. (1997) General mechanisms of metastasis. *Cancer 80*, 1529–1537.

(2) Mareel, M., and Leroy, A. (2003) Clinical, cellular, and molecular aspects of cancer invasion. *Physiol. Rev. 83*, 337–376.

(3) Pollard, T. D. (2007) Regulation of actin filament assembly by Arp2/3 complex and formins. *Annu. Rev. Biophys. Biomol. Struct. 36*, 451–477.

(4) Le Clainche, C., and Carlier, M. F. (2008) Regulation of actin assembly associated with protrusion and adhesion in cell migration. *Physiol. Rev. 88*, 489–513.

(5) Bray, D. (2000) *Cell Movements: From Molecules to Motility*, 2nd ed., Garland Publishing, New York.

(6) Ponti, A., Machacek, M., Gupton, S. L., Waterman-Storer, C. M., and Danuser, G. (2004) Two distinct actin networks drive the protrusion of migrating cells. *Science 305*, 1782–1786.

(7) Medeiros, N. A., Burnette, D. T., and Forscher, P. (2006) Myosin II functions in actin-bundle turnover in neuronal growth cones. *Nat. Cell Biol. 8*, 215–226.

(8) Etienne-Manneville, S. (2004) Actin and microtubules in cell motility: Which one is in control? *Traffic 5*, 470–477

(9) Burnette, D. T., Schaefer, A. W., Ji, L., Danuser, G., and Forscher, P. (2007) Filopodial actin bundles are not necessary for microtubule advance into the peripheral domain of Aplysia neuronal growth cones. *Nat. Cell Biol. 9*, 1360–1369.

(10) Herrmann, H., and Aebi, U. (2000) Intermediate filaments and their associates: multi-talented structural elements specifying cytoarchitecture and cytodynamics. *Curr. Opin. Cell Biol. 12*, 79–90.

(11) Ridley, A., Clark, P. M. (2004) *Cell Motility: From Molecules to Organisms*, John Wiley & Sons, New York.

(12) Etienne-Manneville, S., and Hall, A. (2002) Rho GTPases in cell biology. *Nature 420*, 629–635.

(13) Schulz, W. A. (2007) *Molecular Biology of Human Cancers: An Advanced Student's Textbook*, Springer, New York.

(14) Sapper, A., Wegener, J., and Janshoff, A. (2006) Cell motility probed by noise analysis of thickness shear mode resonators. *Anal. Chem. 78*, 5184–5191.

(15) Tarantola, M., Schneider, D., Sunnick, E., Adam, H., Pierrat, S., Rosman, C., Breus, V., Sonnichsen, C., Basche, T., Wegener, J., and Janshoff, A. (2009) Cytotoxicity of metal and semiconductor nanoparticles indicated by cellular micromotility. *ACS Nano 3*, 213–222.

(16) Tarantola, M., Marel, A.-K., Sunnick, E., Adam, H., Wegener, J., and Janshoff, A. (2010) Dynamics of human cancer cell lines monitored by electrical and acoustic noise analysis. *Integr. Biol. 2*, 139–150.

(17) Tarantola, M., Pietuch, A., Schneider, D., Rother, J., Sunnick, E., Rosman, C., Pierrat, S., Soennichsen, C., Wegener, J., and Janshoff, A. (2011) Toxicity of gold-nanoparticles: Synergistic effects of shape and surface functionalization on micromotility of epithelial cells. *Nanotoxicology 5*, 254–268.

(18) Lovelady, D. C., Friedman, J., Patel, S., Rabson, D. A., and Lo, C. M. (2009) Detecting effects of low levels of cytochalasin B in 3T3 fibroblast cultures by analysis of electrical noise obtained from cellular micromotion. *Biosens. Bioelectron. 24*, 2250–2254.

(19) Wegener, J., Keese, C. R., and Giaever, I. (2002) Recovery of adherent cells after in situ electroporation monitored electrically. *Biotechniques 33*, 348–357.

(20) Wegener, J., Seebach, J., Janshoff, A., and Galla, H. J. (2000) Analysis of the composite response of shear wave resonators to the attachment of mammalian cells. *Biophys. J. 78*, 2821–2833.

(21) Wegener, J., Keese, C. R., and Giaever, I. (2000) Electric cell-substrate impedance sensing (ECIS) as a noninvasive means to monitor the kinetics of cell spreading to artificial surfaces. *Exp. Cell Res. 259*, 158–166.

(22) Schäfer, E., Westendorf, C., Bodenschatz, E., Beta, C., Geil, B., and Janshoff, A. (2011) Shape oscillations of Dictyostelium discoideum cells on ultramicroelectrodes monitored by impedance analysis. *Small 7*, 723–726.

(23) Cooper, M. A., and Singleton, V. T. (2007) A survey of the 2001 to 2005 quartz crystal microbalance biosensor literature: applications of acoustic physics to the analysis of biomolecular interactions. *J. Mol. Recognit. 20*, 154–184.

(24) Marx, K. A., Zhou, T. A., Montrone, A., Schulze, H., and Braunhut, S. J. (2001) A quartz crystal microbalance cell biosensor: detection of microtubule alterations in living cells at nM nocodazole concentrations. *Biosens. Bioelectron. 16*, 773–782.

(25) Marxer, C. M., Coen, M. C., Greber, T., Greber, U. F., and Schlapbach, L. (2003) Cell spreading on quartz crystal microbalance elicits positive frequency shifts indicative of viscosity changes. *Anal. Bioanal. Chem. 377*, 578–586.

(26) Keese, C. R., Wegener, J., Walker, S. R., and Giaever, L. (2004) Electrical wound-healing assay for cells in vitro. *Proc. Natl. Acad. Sci. U.S.A. 101*, 1554–1559.

(27) Ceriotti, L., Ponti, J., Broggi, F., Kob, A., Drechsler, S., Thedinga, E., Colpo, P., Sabbioni, E., Ehret, R., and Rossi, F. (2007) Real-time assessment of cytotoxicity by impedance measurement on a 96-well plate. *Sens. Actuators, B 123*, 769–778.

(28) Braunhut, S. J., McIntosh, D., Vorotnikova, E., Zhou, T., and Marx, K. A. (2005) Detection of apoptosis and drug resistance of human breast cancer cells to taxane treatments using quartz crystal microbalance biosensor technology. *Assay Drug Dev. Technol. 3*, 77–88.

(29) Marx, K. A., Zhou, T., Montrone, A., McIntosh, D., and Braunhut, S. J. (2007) A comparative study of the cytoskeleton binding drugs nocodazole and taxol with a mammalian cell quartz crystal microbalance biosensor: Different dynamic responses and energy dissipation effects. *Anal. Biochem. 361*, 77–92.

(30) Rangan, S. R. S. (1972) New human cell line (Fadu) from a hypopharyngeal carcinoma. *Cancer 29*, 117–121.

(31) Reiss, B., Janshoff, A., Steinem, C., Seebach, J., and Wegner, J. (2003) Adhesion kinetics of functionalized vesicles and mammalian cells: a comparative study. *Langmuir 19*, 1816–1823.

(32) Giaever, I., and Keese, C. R. (1991) Micromotion of mammalian-cells measured electrically. *Proc. Natl. Acad. Sci. U.S.A. 88*, 7896–7900.

(33) Janshoff, A., Kunze, A., Michaelis, S., Heitmann, V., Reiss, B., and Wegener, J. (2010) Cell Adhesion Monitoring Using Substrate-Integrated Sensors. *J. Adhes. Sci. Technol. 24*, 2079–2104.

(34) Lo, C. M., Keese, C. R., and Giaever, I. (1995) Impedance analysis of MDCK cells measured by electric cell-substrate impedance sensing. *Biophys. J. 69*, 2800–2807.

(35) Rodahl, M., Hook, F., Fredriksson, C., Keller, C. A., Krozer, A., Brzezinski, P., Voinova, M., and Kasemo, B. (1997) Simultaneous frequency and dissipation factor QCM measurements of biomolecular adsorption and cell adhesion. *Faraday Discuss.* 229–246.

(36) Rodahl, M., and Kasemo, B. (1996) A simple setup to simultaneously measure the resonant frequency and the absolute dissipation factor of a quartz crystal microbalance. *Rev. Sci. Instrum. 67*, 3238–3241.

(37) Sauerbrey, G. (1959) Verwendung Von Schwingquarzen Zur Waegung Duenner Schichten Und Zur Mikrowaegung. *Z. Phys. 155*, 206–222.

(38) Janshoff, A., Galla, H. J., and Steinem, C. (2000) Piezoelectric mass-sensing devices as biosensors: An alternative to optical biosensors? *Angew Chem., Int. Ed. 39*, 4004–4032.

(39) Bandey, H. L., Martin, S. J., Cernosek, R. W., and Hillman, A. R. (1999) Modeling the responses of thickness-shear mode resonators under various loading conditions. *Anal. Chem. 71*, 2205–2214.

(40) Li, F., Wang, J. H.-C., and Wang, Q.-M. (2008) Thickness shear mode acoustic wave sensors for characterizing the viscoelastic properties of cell monolayer. *Sens. Actuators, B 128*, 399–406.

(41) Rotsch, C., and Radmacher, M. (2000) Drug-induced changes of cytoskeletal structure and mechanics in fibroblasts: An atomic force microscopy study. *Biophys. J. 78*, 520–535.

(42) Cooper, J. A. (1987) Effects of cytochalasin and phalloidin on actin. *J. Cell Biol. 105*, 1473–1478.

(43) Kovacs, M., Toth, J., Hetenyi, C., Malnasi-Csizmadia, A., and Sellers, J. R. (2004) Mechanism of blebbistatin inhibition of myosin II. *J. Biol. Chem. 279*, 35557–35563.

(44) Gabriele, S., Benoliel, A. M., Bongrand, P., and Theodoly, O. (2009) Microfluidic investigation reveals distinct roles for actin cytoskeleton and myosin II activity in capillary leukocyte trafficking. *Biophys. J. 96*, 4308–4318.

(45) Martens, J. C., and Radmacher, M. (2008) Softening of the actin cytoskeleton by inhibition of myosin II. *Pfluegers Arch. 456*, 95–100.

(46) Balland, M., Richert, A., and Gallet, F. (2005) The dissipative contribution of myosin II in the cytoskeleton dynamics of myoblasts. *Eur. Biophys. J. 34*, 255–261.

(47) Schiff, P. B., Fant, J., and Horwitz, S. B. (1979) Promotion of microtubule assembly in vitro by taxol. *Nature 277*, 665–667.

(48) Liu, Q. J., Yu, J. J., Xiao, L., Tang, J. C. O., Zhang, Y., Wang, P., and Yang, M. (2009) Impedance studies of bio-behavior and chemosensitivity of cancer cells by micro-electrode arrays. *Biosens. Bioelectron. 24*, 1305–1310.

(49) Arndt, S., Seebach, J., Psathaki, K., Galla, H. J., and Wegener, J. (2004) Bioelectrical impedance assay to monitor changes in cell shape during apoptosis. *Biosens. Bioelectron. 19*, 583–594.

(50) Fenteany, G., and Zhu, S. T. (2003) Small-molecule inhibitors of actin dynamics and cell motility. *Curr. Top. Med. Chem. 3*, 593–616.

(51) Tsai, M. A., Waugh, R. E., and Keng, P. C. (1998) Passive mechanical behavior of human neutrophils: Effects of colchicine and paclitaxel. *Biophys. J. 74*, 3282–3291.

(52) Pesen, D., and Hoh, J. H. (2005) Micromechanical architecture of the endothelial cell cortex. *Biophys. J. 88*, 670–679.

(53) Myers, J. N., Greenberg, J. S., Mo, V., and Roberts, D. (2001) Extracapsular spread: A significant predictor of treatment failure in patients with squamous cell carcinoma of the tongue. *Cancer 92*, 3030–3036.

(54) Rosenthal, E. L., and Matrisian, L. M. (2006) Matrix metalloproteases in head and neck cancer. *Head Neck-J. Sci. Spec. 28*, 639–648.